NASA TECHNICAL MEMORANDUM

NASA TM-78885

NASA TM-78885

(NASA-TM-78885) THREE-DIMENSIONAL EFFECTS ON PURE TONE FAN NOISE DUE TO INFLOW DISTORTION (NASA) 26 p HC A03/MF A01 CSCL 20A

N78-24898

Unclas
G3/71 16803

THREE-DIMENSIONAL EFFECTS ON PURE TONE FAN NOISE DUE TO INFLOW DISTORTION

by Hiroshi Kobayashi
Lewis Research Center
Cleveland, Ohio 44135

TECHNICAL PAPER to be presented at the
Eleventh Fluid and Plasma Dynamics Conference
sponsored by the American Institute of Aeronautics and Astronautics
Seattle, Washington, July 10-12, 1978

THREE-DIMENSIONAL EFFECTS ON PURE TONE FAN NOISE DUE TO INFLOW DISTORTION

Hiroshi Kobayashi*
National Aeronautics and Space Administration
Lewis Research Center
Cleveland, Ohio 44135

ORIGINAL PAGE IS OF POOR QUALITY

E-9618

Abstract

For the prediction of fan noise, the two-dimensional method has been used in many cases. However, the accuracy of the two-dimensional method needs to be assessed against three-dimensional effects. Therefore, two-dimensional, quasi three-dimensional and three dimensional theories for the prediction of pure tone fan noise due to the interaction of inflow distortion with a subsonic annular blade row have been studied with the aid of an unsteady three-dimensional lifting surface theory developed by Namba.[1,2] The present study also examines the effects of compact and noncompact source distributions on pure tone fan noise in an annular cascade. Numerical results show that the strip theory and quasi three-dimensional theory are reasonably adequate for fan noise prediction. The quasi three-dimensional method is more accurate for acoustic power and modal structure prediction with an acoustic power estimation error of about ±2 dB. This accuracy seems to be affected not by the subresonance or super-resonance status of the acoustic modes, but by the reduced frequency of the inflow-distortion and by the inflow distortion radial distribution. Also, the compact source prediction is different from the noncompact source prediction by as much as 15 dB in upstream radiation cases and by as much as 6 dB in downstream cases, depending on reduced frequency and interblade phase.

Introduction

A major source of fan noise is unsteady flows interacting with blades and vanes. These unsteady flows are inlet distortions[3-7] such as atmospheric turbulence,[8] cross-wind effects,[9] static test installation wakes, fan inlet boundary layers and the ground vortices that are apparent during many static test conditions, all of which can produce a significant levels of noise with a fan or a turbofan engine. Because these inflow conditions can vary during the course of a test program, and can vary significantly between static testing and forward flight of an engine,[10] the evaluation of noise reduction features using static testing and the extrapolation to flight of static noise levels is extremely complicated and may prove erroneous.

For flyover noise prediction, source noise error is only a part of the problem since atmospheric propagation effects and installation effects also appear to contribute significantly. However, the study of fan noise sources is an important part of this problem, and knowledge of the importance and strengths of possible sources of unsteady flows described above is particularly important in selecting a facility for simulating flight behavior statically. The degree of importance of these unsteady flows will depend on the particular fan stage and unsteady flow structure. It is therefore important to correlate the results of various fan noise calculations with the existing experimental model data and thereby define the interplay of scales and intensities in determining noise levels and to suggest the most fruitful inflow control strategies. These calculations can also provide information about fan noise modal structure for acoustic suppressor design.[11]

Many theoretical studies of fan noise have been based on two-dimensional linear cascade models[4-8,12-14] that have made clear the fundamental features of the sound generation process and have shown the effect of the various factors that influence sound source noise. However, it has not been made clear over what range of conditions these current two-dimensional theories are able to predict the unsteady blade forces and the sound field for the case of a three-dimensional annular blade row and for complicated inflow-distortions. The two-dimensional problem is easier to handle and to obtain numerical results for; however, comparison of two and three-dimensional results is needed over a wide range of parameters and inflow conditions.

The available theoretical results on unsteady blade forces for a single airfoil in an oblique gust[15] show that the unsteady lift force amplitude decreases as the spanwise wave number of the gust increases. We can infer then, that three-dimensional effects will play an important role on fluctuating blade forces in the case of interaction with an inflow distortion of large radial extent. As Tyler and Sofrin[16] pointed out, the interaction field generates many modes with various circumferential and radial mode numbers, and whether these modes propagates or decay depends strongly on the three-dimensional duct cutoff phenomena. Therefore, the role of three-dimensional effects in the prediction of unsteady blade forces and acoustic power and acoustic modal structure has to be clarified.

A theoretical analysis of the unsteady force and the total acoustic power in a three-dimensional annular cascade was carried out by Namba.[1] Several of the three-dimensional effects on unsteady forces and acoustic power were obtained. However, in his numerical calculations, the reduced frequency is treated as a constant value, without regard to inflow distortion circumferential mode number and the rotational speed of rotor, and so correct numerical results for rotor-inflow distortion interaction noise are not presented. Also, in his calculation, the circumferential and radial distributions of the inflow distortion were limited to the case of simple harmonic distortion.

Therefore, in this paper, a theoretical analysis of pure tone fan noise generated by inflow distortion-rotor interaction was carried out with the aid of the three-dimensional unsteady lifting surface theory developed by Namba,[1,2] accepting as input various inflow distortions, in order to predict the forward and aft radiated pure tone energy and the modal energy distribution. Special empha-

*National Aerospace Laboratory, Tokyo, Japan; NRC - NASA Lewis Research Associate.

STAR Category 71
AIAA Paper No. 78-1120

sis is placed upon the clarification of the accuracy of available two-dimensional theory for the prediction of pure tone fan noise due to the interaction of inflow distortion with a subsonic annular blade row. For this study, three-dimensional calculations, two-dimensional calculations (strip theory) and quasi three-dimensional calculations are carried out and compared. In the quasi three-dimensional calculation, two-dimensional chordwise dipole distributions at several radial positions are resolved into Fourier-Bessel dipole distributions on an annular blade row, and then, with this dipole distribution, the pure tone fan energy and modal structure in a three-dimensional annular duct are calculated. In addition, the effects of compact and noncompact sources in an annular blade row on pure tone fan noise are also studied.

The procedure and assumptions introduced in the present study are described as follows. The theoretical model consists of a single three-dimensional annular cascade rotating at constant angular velocity in an annular rigid-wall duct of infinite axial extent. Thus, the duct end reflection, the effect of upstream or downstream blade rows, and the effects of duct area variation are not considered. These effects except for the last one, could be included in the solution procedure of the present study. The undisturbed flow is uniform axially and the relative velocity over the whole blade span is limited to the subsonic range. In order to make the problem tractable, linearized theory is adopted; that is, not only fluctuating quantities due to sound but also those due to the inflow distortion convected with the basic flow, are assumed to be small quantities of the first order in comparison to the mean pressure or the main stream velocity, respectively.

The calculation procedure is as follows. First, the periodic velocity fluctuations at the rotor blades due to the inflow distortion are obtained. Second, in order to cancel the fluctuating component of the velocity normal to the airfoils, acoustic dipoles are assumed to be distributed over the surface of the rotor blade. Fluctuating pressure and velocity fields induced by the rotor blades are expressed through a kernel function in terms of the dipole distribution on a blade. The spanwise distribution of acoustic dipoles is given as a sum of acoustic radial mode components and the kernel function is resolved into the corresponding modal components. Finally, the boundary condition that the fluctuating velocity normal to the aerofoil should vanish at each blade surface position is introduced. By solving the resulting integral equation numerically, we obtained the dipole distributions, which are then used to calculate the sound pressure in the far field. Thus, the pure tone acoustic power and modal structure upstream and downstream of the rotor are obtained. The inflow distortion is resolved into its Fourier-Bessel components, and then the effects of each inflow distortion component on the acoustic power is superimposed to obtain the total pure tone acoustic power. It is worth noting that the same acoustic mode can be generated by all the inflow distortion components that have the same circumferential mode number, even though their radial mode numbers are different.

Analytical Model

Fluctuating Pressure Induced by Rotor Blades Row

The theoretical model considered here consists of a single annular blade row with N blades rotating at a constant angular velocity ω_T^* in an annular rigid walled duct of infinite axial extent (Fig. 1). The fluid flow is composed of an undisturbed flow with a uniform axial velocity W_a and small fluctuating flows due to the rotor blades and inflow distortion. The flow is inviscid, of uniform entropy and has no thermal conductivity. The fluctuation induced by the rotor is assumed to be isentropic. The fluctuations of the fluid flow are small compared with the undisturbed flow. It is also assumed that the fluid velocity relative to the blades is subsonic along the whole span and that the blades have no steady load.

A cylindrical polar coordinate system is used with axes (r,θ,z) fixed to the rotor as shown in Fig. 1. The radial and axial coordinates r and z are normalized with respect to the radius r_T^* at the blade tip. The dimensionless time t is correspondingly scaled with respect to r_T^*/W_a. Then in accordance with the assumptions given above, the continuity, momentum and energy equations are combined to give the following linearized equation[2,17] for the fluctuating pressure p

$$\left[\nabla^2 - \left(\frac{1}{a_o^2}\right)\frac{D^2}{Dt^2}\right] \cdot P = 0, \tag{1}$$

where

$$\nabla^2 - \frac{1}{a_o^2}\frac{D^2}{Dt^2} = \left(1 - M_a^2\right)\frac{\partial^2}{\partial z^2} + \frac{1}{r^2}\left(1 - M_a^2\omega_T^2 r^2\right)\frac{\partial^2}{\partial\theta^2}$$

$$- 2M_a^2\omega_T\frac{\partial^2}{\partial z\,\partial\theta} + \frac{\partial^2}{\partial r^2} + \frac{1}{r}\frac{\partial}{\partial r} - 2M_a^2\frac{\partial^2}{\partial z\,\partial t}$$

$$- 2M_a^2\omega_T\frac{\partial^2}{\partial\theta\,\partial t} - M_a^2\frac{\partial^2}{\partial t^2} \tag{2}$$

This equation is nothing other than the acoustic wave equation in the rotor-fixed coordinate and its solution must satisfy the boundary condition requiring that the radial velocity vanish on the rigid wall surfaces at the hub and tip radii. In the present approximation, a rigid, thin airfoil placed in the periodically fluctuating velocity field is directly equivalent to a sheet of acoustic dipoles, or, in other words, an unsteady lifting surface. Therefore, a rotor blade row can be represented by N acoustic dipole sheets with the dipole axes normal to the surface. The N acoustic dipole sheets have a constant interblade phase difference and are circumferentially equally spaced at the locations $(\rho, \varphi + 2j\pi/N, \zeta)(j = 0, 1, 2, \ldots, N - 1)$. The fluctuating pressure due to the rotor blade row can be expressed in the form

$$P(r,\theta,z) = \sum_{q=-\infty}^{\infty}\sum_{p=-\infty}^{\infty}\tilde{P}_{q,p}(r,\theta,z)\,e^{i\omega t}, \tag{3}$$

where

$$\tilde{P}_{q,p}(r,\theta,z)$$

$$= \int_h^1 d\rho \int_{-C_a/2}^{C_a/2} \Delta P_{q,p}(\rho,\zeta) KP(r,\theta,z,\rho,\zeta,q) d\zeta', \quad (4)$$

$$KP(r,\theta,z,\rho,\zeta,q)$$

$$= \frac{1}{\Lambda(\rho)} \left[\frac{1}{\sqrt{1+\omega_T^2\rho^2}} \left(-\omega_T \rho \frac{\partial}{\partial\zeta} + \frac{1}{\rho}\frac{\partial}{\partial\varphi} \right) \times \tilde{P}_c(r,\theta,z/\rho,\varphi,\zeta) \right]_{\varphi=\omega_T z'} \quad (5)$$

$$\Lambda(\rho) = \left(1+\omega_T^2\rho^2\right)\left[\rho^2\left(1+\omega_T^2\right)\right] \quad (6)$$

$$\tilde{P}_c(r,\theta,z/\rho,\varphi,z)$$

$$= \frac{N}{4\pi\beta_a^2} \sum_{\nu=-\infty}^{\infty} \sum_{l=0}^{\infty} \frac{1}{\Omega_{n,l}} R_n(k_{n,l}\cdot r)\, R_n(k_{n,l}\cdot\rho)$$

$$\times \exp\left[in(\theta-\varphi) + i(n\omega_T+\omega)(z-\zeta)M_a^2/\beta_a^2 - \Omega_{n,l}|z-\zeta|\right] \quad (7)$$

$\Delta P_{q,p}(\rho,\zeta)\cdot e^{i\omega t}$ denotes the pressure jump across the blade surface caused by (q,p) mode components of the inflow distortion, where q and p are, respectively, a circumferential mode number and a radial mode number of the inflow distortion. C_a denotes the axial chord length of the blades, which is assumed constant along the span. $\omega C_a = C_a^*(q\omega_T^*)r_T^*/\bar{W}_a$ is the reduced frequency, $M_a = \bar{W}_a/a_0$ is the axial Mach number, $\beta_a^2 = 1 - M_a^2$ is the Prandtl-Glauert parameter and further $\Omega_{n,l}$ is defined by

$$\Omega_{n,l}^2 = \left[k_{n,l}^2 - (n+q)^2\omega_T^2 M_a^2/\beta_a^2\right]/\beta_a^2 \quad (8)$$

$R_n(k_{n,l}\cdot r)$ and $k_{n,l}$ are respectively the normalized radial eigen-function and its eigenvalue, where $n(=\nu N+\sigma)$ and l denote the circumferential mode number and the radial mode number, respectively, of a pressure wave.

The factor $\Omega_{n,l}$ is either a positive real or a positive imaginary number. Evidently the modes corresponding to real $\Omega_{n,l}$ are the cutoff waves that decay *in the far-field*, while the modes associated with imaginary values of $\Omega_{n,l}$ are the cut-on waves that propagate without decaying. The critical values of ν and l depend upon the axial Mach number M_a, the rotational speed of rotor ω_T, the hub-tip ratio h and the circumferential mode number of the inflow distortion q, but not on the radial mode number of inflow distortion p.

Equation (4) can be written in the Fourier-Bessel double series from as follows:

$$\tilde{P}_{q,p}(r,\theta,z) = -\frac{N}{4\pi\beta_a^2} \int_{-C_a/2}^{C_a/2} \sum_{\nu=-\infty}^{\infty} \sum_{l=0}^{\infty} R_n(k_{n,l}\cdot r)$$

$$\times \exp\left[in(\theta-\omega_T\zeta) + i(n\omega_T+\omega)(z-\zeta)M_a^2/\beta_a^2 - \Omega_{n,l}|z-\zeta|\right]$$

$$\times \left\{ \frac{1}{\Omega_{n,l}} \left[G_{n,l}(\zeta,q,p)\frac{M_a^2}{\beta_a^2}\omega_T \times (n\omega_T+\omega) - n\cdot F_{n,l}(\zeta,q,p) \right] - G_{n,l}(\zeta,q,p)\cdot\omega_T\cdot \mathrm{sgn}(z-\zeta) \right\} d\zeta \quad (9)$$

where $G_{n,l}(\zeta,q,p)$ and $F_{n,l}(\zeta,q,p)$ are the blade force coefficients defined by

$$\begin{bmatrix} G_{n,l}(\zeta,q,p) \\ F_{n,l}(\zeta,q,p) \end{bmatrix} = \int_h^1 \Delta P_{q,p}(\rho,\zeta)\frac{1}{\Lambda(\rho)}\cdot R_n(k_{n,l}\cdot\rho)\begin{bmatrix} \rho \\ 1/\rho \end{bmatrix} d\rho \quad (10)$$

which is equivalent to

$$\Delta P_{q,p}(\rho,\zeta) = \Lambda(\rho)\sum_{l=0}^{\infty} G_{n,l}(\zeta,q,p)\cdot R_n(k_{n,l}\cdot\rho)$$

$$= \rho^2\,\Lambda(\rho)\sum_{l=0}^{\infty} F_{n,l}(\zeta,q,p)\cdot R_n(k_{n,l}\cdot\rho) \quad (11)$$

Equation (9) expresses the fluctuating pressure as a super-position of an infinite number of pressure modes which are characterized by the circumferential mode number $n(=\nu N+\sigma)$ and the radial mode number l. Expression (9) is convenient for a modal analysis of the pressure field, but it is inconvenient for evaluating the near field pressure for two reasons. First, the series expansion with respect to the circumferential wave number n is nonuniformly convergent at the blade surface. Second, it involves too many blade force coefficients $G_{n,l}(\zeta,q,p)$ and $F_{n,l}(\zeta,q,p)$ $(l = 0, 1, 2, \ldots, \nu = 0, 1, 2, \ldots)$ which are also functions of the axial position ζ. These difficulties, which may be crucial, especially in a case where the unsteady lift force distribution $\Delta P_{q,p}(\rho,\sigma)$ cannot be specified a priori, were eliminated by the method developed by Namba.[2] The method is founded upon approximating $R_n(k_{n,l}\cdot r)$ by a finite series of the $R_o(k_{o,l}\cdot r)$ in the form

$$R_n(k_{n,l}\cdot r) = \sum_{k=0}^{L-1} B_{n,l,k}\, R_o(k_{o,k}\cdot r). \quad (12)$$

The number L of retained terms should be appropriately large. With this method, equation (4) can be rearranged to obtain

ORIGINAL PAGE IS
OF POOR QUALITY

$$\tilde{P}_{q,p}(r,\theta,z)$$

$$= -\frac{N}{4\pi\beta_a^2}\int_{-C_a/2}^{C_a/2}\sum_{k=0}^{L-1} G_{o,k}(\zeta,q,p)\cdot KP_k(r,\theta,z/\zeta,q)\,d\zeta. \tag{13}$$

The kernel function $KP_k(r,\theta,z/\zeta,q)$ is governed by the parameters N, ω_T, h, q, M_a, ω, σ and L. KP_k can be resolved into three parts; $KP_k^{(P)}$ (propagating part), $KP_k^{(S)}$ (singular part), and $KP_k^{(R)}$ (regular part).

Fluctuating Velocity Induced by Rotor Blade Row

The fluctuating velocity $q(r,\theta,z)\,e^{i\omega t}$ can be obtained by integrating the linearized Euler's equation of motion as follows;

$$q(r,\theta,z)$$

$$= -\frac{1}{\rho_o Q}\,e^{-i\omega z}\int_{-\infty}^{z} e^{i\omega z}\left[\nabla P(r,\theta,z)\right]_{\theta=\theta_o+\omega_T z} dz, \tag{14}$$

where ρ_o denotes the fluid density in the undisturbed state and $Q = \overline{W}_a\cdot\sqrt{1+\omega_T^2 r^2}$ is the velocity of the undisturbed fluid relative to the blades. Combining equations (4) and (14) leads to the expression of the fluctuating velocity in terms of the blade force mode coefficients. Then the upwash component $q(r,\theta,z)\,e^{i\omega t}$ can be expressed in the following form

$$q_\tau(r,\theta,z) = -\frac{1}{\rho_o Q}\frac{N}{4\pi}$$

$$\times\sum_{q=-\infty}^{\infty}\sum_{p=-\infty}^{\infty}\int_{-C_a/2}^{C_a/2}\sum_{k=0}^{L-1} G_{o,k}(\zeta,q,p)$$

$$\cdot KT_k(r,\theta,z/\zeta,q)\,d\zeta. \tag{15}$$

The upwash kernel function contains parameters of N, h, q, ω_T, σ, and L. The detailed expression for the kernel function KT_k are given in Appendix I. As shown, KT_k is divided into three parts the same as KP_k; the propagating part $KT_k^{(P)}$, the singular part $KT_k^{(S)}$, and the regular part $KT_k^{(R)}$. The singular part $KT_k^{(S)}$ possesses singularities at the lifting surface.

Inflow Distortion

In this paper the inflow distortion is assumed to have only an axial velocity component (see Fig. 2). If a Fourier-Bessel analysis of the arbitrary shapes of inflow distortion is carried out, the following axial component of external fluctuating velocity is obtained.

$$w_{e,a}(r,\theta,z,t) = \epsilon_a\cdot\overline{W}_a\sum_{q=-\infty}^{\infty} A_q(r)\cdot e^{-iq(\theta-\omega_T t)} \tag{16-1}$$

$$= \epsilon_a\cdot\overline{W}_a\sum_{q=-\infty}^{\infty}\sum_{p=-\infty}^{\infty} B_{q,p}\cdot R_q(k_{q,p}\cdot r)$$

$$\times\, e^{-iq(\theta-\omega_T t)} \tag{16-2}$$

where q and p are respectively the circumferential mode number and radial mode number. ϵ_a denotes a small quantity which is the ratio of the external fluctuating velocity to the basic flow velocity. Since the upwash component of external fluctuating velocity is given by

$$q_{\tau,w} = -w_{e,a}\cdot\omega_T\cdot r\Big/\sqrt{1+\omega_T^2 r^2} \tag{17}$$

then, one can express the upwash component of the external fluctuating velocity on a blade surface $\theta = \omega_T z$ by

$$\left[q_{\tau,w}\right]_{\theta=\omega_T z} = -w_{e,a}\cdot e^{-iq\omega_T(z-t)}\frac{\omega_T r}{\sqrt{1+\omega_T^2 r^2}} \tag{18}$$

One easily sees that the reduced frequency ωC_a and the interblade phase angle $2\pi\sigma/N$ of inflow distortion sensed by the rotor blades are given by

$$\omega\cdot C_a = q\cdot C_a\cdot\omega_T \quad\text{and}\quad \sigma = mN - q \tag{19}$$

where the integer m is chosen so that $|2\pi\,\sigma/N|\le\pi$ is satisfied. It follows from equation (16) that the Fourier coefficient $B_{q,p}$ can be determined from the axial distortion velocity $w_{e,a}$ by the relation

$$B_{q,p} = \frac{1}{2\pi}\int_0^{2\pi}\int_h^1 r\cdot R_q(k_{q,p}\cdot r)\frac{w_{e,a}(r,\hat{\theta})}{\epsilon_a\cdot\overline{W}_a}e^{iq\hat{\theta}}\,dr\,d\theta \tag{20}$$

It is convenient to suppose that the distortion velocity can be expressed as the product[6]

$$\frac{w_{e,a}(r,\hat{\theta})}{\epsilon_a\cdot W_a} = F_1(r)\cdot\Theta_1(\hat{\theta}) \tag{21}$$

then

$$B_{q,p} = a_q\cdot b_p \tag{22}$$

where

$$a_q = \frac{1}{2\pi}\int_0^{2\pi} e^{-iq\hat{\theta}}\cdot\Theta_1(\hat{\theta})\,d\hat{\theta} \tag{23}$$

and

$$b_p = \int_h^1 r\cdot R_q(k_{q,p}\cdot r)\cdot F_1(r)\,dr \tag{24}$$

When the inflow distortion can be represented by N Gaussian profiles (for $N = 1, 2, \ldots$) in the circumferential direction.

$$\theta_1(\theta) = \exp\left[\frac{-\left(\frac{\theta}{2\pi} - \frac{1+2j}{2\pi}\right)^2}{(\theta_2)^2}\right]\left\{\begin{array}{l}\left[\frac{j}{N}2\pi < \theta < \frac{j+1}{N}2\pi\right. \\ \text{for } j = 0, 1, 2, \ldots, N-1\end{array}\right. \tag{25}$$

We find that

$$a_q = \begin{cases} \sqrt{\pi}\cdot N\cdot\theta_2\cdot e^{-\frac{i\pi}{N}q}\cdot e^{-\pi^2 q^2\theta_2^2}\left[\mathrm{Re}\cdot \mathrm{erf}\left(\frac{1}{2N\theta_2} + iq\pi\cdot\theta_2\right)\right] \\ 0 \text{ otherwise} \qquad \text{for } q = 0, \pm N, \pm 2N, \ldots \end{cases} \tag{26}$$

Determination of Acoustic Dipole Distribution

In the previous sections, the fluctuating pressure and velocity induced by the rotor blades have been represented in terms of the acoustic dipole distribution, namely, the unsteady lifting pressure $\Delta P(r,z)\, e^{i\omega t}$ on the blades. The acoustic dipole distribution must be determined so that the normal component of the relative fluid velocity should vanish at the blade surfaces. Therefore, the upwash component of the external fluctuating velocity $q_{\tau W}$ must be cancelled by the induced upwash velocity $q_\tau(r,\theta,z)\, e^{i\omega t}$ at the blade surfaces; that is, for $|z| \leq C_a/2$,

$$q_\tau(r,\omega_r z, z)\, e^{i\omega t} + \left[q_{\tau W}\right]_{\theta=\omega_r z} = 0 \tag{27}$$

Combining equation (27) with equations (15) and (18), we obtain an integral equation for the unknown acoustic dipole $G_{o,k}(\zeta,q,p)$ in the form

$$\sum_q\sum_p \frac{N}{8\pi}\left[\int_{-C_a/2}^{C_a/2}\sum_{m=0}^{L-1}\tilde{G}_{o,m}(\zeta,q,p)\cdot KT_m(r,\omega_r z, z-\zeta,q)\, d\zeta - B_{q,p}\cdot R_q(k_{q,p}\cdot r)\, r\omega_r\cdot e^{-iq\omega_r z}\right] = 0 \tag{28}$$

where

$$\tilde{G}_{o,m}(\zeta,q,p) = G_{o,m}(\zeta,q,p)\Big/\frac{\varepsilon_a\cdot\rho_o\overline{W}_a^2}{2} \tag{29}$$

We adopt the following method to obtain acoustic dipole distribution from equation (28). The coordinates ζ and z are transformed into angle variables φ_1 and φ_2 such that

$$\begin{aligned}\zeta &= -(C_a/2)\cdot\cos\varphi_1 \\ z &= -(C_a/2)\cdot\cos\varphi_2\end{aligned} \tag{30}$$

where

$$\begin{aligned}\varphi_1 &= (r-1)\pi/M, \\ \varphi_2 &= (2r-1)\pi/2M\end{aligned} \qquad (r = 1, 2, \ldots, M) \tag{31}$$

M is the number of chordwise acoustic dipole points and is also the chordwise boundary points on a blade. $G_{o,k}(\zeta,q,p)$ are represented by

$$\tilde{G}_{o,k}(\zeta,q,p) = \tilde{G}^*_{ok}(\varphi_1,q,p)\Big/\left(\frac{C_a}{2}\sin\varphi_1\right) \tag{32}$$

The quantity $\tilde{G}^*_{ok}(\varphi_1,q,p)$ is calculated from equation (28) by a collocation method. The solution is assumed to satisfy a Kutta condition at the trailing edge i.e., $G^*_{o,k}(\pi,q,p) = 0$.

Pure Tone Acoustic Power

The pure tone fan noise is composed of a finite number of propagating pressure modes which depend on the parameters ν, l, q, ω_r, M_a and N. Using equation (3), we can obtain the expression for sound pressure

$$P_\pm(r,\theta,z) = \frac{\varepsilon_a\rho_o\overline{W}_a^2}{2}\sum_q\sum_{n=n_1}^{n_2}\sum_{l=0}^{l_e} R_n(k_{n,l}\cdot r)\cdot e^{i(n\theta+\alpha_\pm z)} \times HP_\pm(n,l,q)\cdot e^{i(\nu+m)N\omega_r t} \tag{33}$$

Here the auffixes + and - denote the sound waves propagating forward (downstream) and backward (upstream) respectively, and $HP_\pm(n,l,q)$ denotes the nondimensional pressure amplitude in the (n,l) acoustic mode, which is given in the noncompact source case by

$$HP_\pm(n,l,q) = -\frac{N}{4\pi\beta_a^2}\sum_{k=0}^{L-1}\left[\frac{\omega_r\alpha_\pm}{\Omega_{n,l}}B_{l,n,k} - \frac{n}{\Omega_{n,l}}C_{n,l,k}\right] \times\int_{-C_a/2}^{C_a/2}\sum_p\tilde{G}_{o,k}(\zeta,q,p)\cdot\exp\left[-i(\alpha_\pm + n\omega_r)\cdot\zeta\right] d\zeta \tag{34-1}$$

while in the case of a compact source

$$HP_\pm(n,l,q) = -\frac{N}{4\pi\beta_a^2}\sum_{k=0}^{L-1}\left[\frac{\omega_r\alpha_\pm}{\Omega_{n,l}}B_{n,l,k} - \frac{n}{\Omega_{n,l}}C_{n,l,k}\right] \times\int_{-C_a/2}^{C_a/2}\sum_p\tilde{G}_{o,k}(\zeta,q,p)\, d\zeta \tag{34-2}$$

Further $\alpha_\pm$, given by

$$\alpha_\pm = \frac{M_a^2}{\beta_a^2}(n\omega_T + \omega) \mp |\Omega_{n,l}| = \frac{M_a^2}{\beta_a^2}(n+q)\omega_T \mp |\Omega_{n,l}| \tag{35}$$

denotes the axial wave number per length r_T^*.

Corresponding to each circumferential mode number of inflow distortion, the circumferential acoustic mode numbers n (namely ν) which can propagate are decided with equation (8). The pure tone harmonic number corresponding to each mode number n is not ν, but $\nu+m$, where m is obtained from equation (19). The inflow distortion radial mode number p has no influence on whether or not the fluctuating pressure caused by the inflow distortion-rotor interaction can propagate, but it affects the amplitude of pure tone fan noise. Therefore, we need to sum all sound pressures corresponding to each circumferential mode number q and radial mode number p of the inflow distortion, in order to obtain the pure tone fan noise caused by the arbitrary shaped inflow distortion.

From equation (15), we can get the expression of the propagating axial fluctuating velocity in the following form,

$$w_{a,p}(r,\theta,z) = -\frac{\overline{W}_a}{2}\sum_q \sum_{n=n_1}^{n_2} \sum_{l=0}^{l_e} \frac{\alpha_\pm}{\alpha_\pm + (n\omega_T + \omega)} \cdot R_n(k_{n,l}\cdot r)$$

$$\times\ e^{i(n\theta+\alpha_\pm z)} \cdot HP_\pm(n,l,q)\ e^{i(\nu+m)N\omega_T t} \tag{36}$$

Following Morfey's approach,[18] the axial component of the sound intensity $I_z^{j\pm}$ of pure tone fan noise (harmonic number $j = 1, 2, 3, \ldots$) referred to the duct-fixed coordinate system is obtained in the form

$$I_z^{j\pm} = \left(1 + M_a^2\right)\langle p^j \cdot w^j\rangle + \left(\overline{W}_a^2/\rho_o a_o^2\right)\left\langle p^{j\,2}\right\rangle + \rho_o \overline{W}_a \left\langle w^{j\,2}\right\rangle \tag{37}$$

$$= \sum_q \sum_{n=n_1}^{n_2} \sum_{l=0}^{l_e} c_a \cdot \rho_o \overline{W}_a^3 \cdot R_n^2(k_{n,l}\cdot r)\ (n\omega_T + \omega)\ \beta_a^2$$

$$\times\ |\Omega_{n,l}|\,|HP_\pm(n,l,q)|^2 \big/ 8\left[\alpha_\pm + (n\omega_T + \omega)\right]^2 \tag{38}$$

where $\langle\ \rangle$ denotes the time average value. Also, of course, p and W in equation stand for the real parts of the original complex forms of p and W.

Therefore, the dimensionless acoustic power $E_\pm^j$ with respect to each pure tone fan harmonic (for example $j = +m=\pm 1$ corresponds to 1st harmonic) is obtained by

$$E_\pm^j = \int_h^1 r\cdot dr \int_0^{2\pi} I_z^{j\pm}\, d\theta \Big/ \left(\frac{\pi}{4}\,\rho_o \overline{W}_a^3 \epsilon_a^2 r_T^{*2}\right)$$

$$= \sum_q \sum_{n=n_1}^{n_2} \sum_{l=0}^{l_e} EI_\pm^j(n,l,q) \tag{39}$$

where

$EI_\pm^j(n,l,q)$

$$= |HP_\pm(n,l,q)|^2\, \beta_a^2 (n\omega_T + \omega)\,|\Omega_{n,l}| \big/ (\alpha_\pm + n\omega_T + \omega)^2 \tag{40}$$

$EI_\pm^j(n,l,q)$ is the modal component of the dimensionless acoustic power.

Two-Dimensional Theory (Strip Theory) and Quasi Three-Dimensional Theory

A two-dimensional cascade calculation is obtained as the limit of large cylinder radii. In the notation of this paper, this limit corresponds to $h \to 1$ and $N \to \infty$ simultaneously, while keeping $2\pi/\left(NC_a\sqrt{1+\omega_T^2}\right) = \hat{C}$ constant at each radius of the annular blade row and q/N = constant, where $\hat{C}$ is the pitch-chord ratio and q/N is the ratio of inflow distortion circumferential wave length to cascade pitch.

In the quasi three-dimensional method, first, the chordwise unsteady force distributions (namely, acoustic dipole chordwise distribution) are calculated at L numbers of radial positions from hub to tip using the two dimensional cascade calculation. Second, those dipole distributions on a blade are resolved into Fourier-Bessel form with equation (11) and then the pure tone fan noise and modal structure in three-dimensional annular cascade are computed from equations (39) and (40).

Numerical Results

The numerical calculations are carried out in this paper for two different rotor configurations. Their geometric parameters are given in Table I. The fan denoted case No. 1 has a high tip-speed and a large number of blades, while the No. 2 case fan has low tip-speed and a small blade number. Under these conditions, the pitch-chord ratio S, the stagger angle γ, and the ratio of the relative flow-velocity to the axial flow velocity $Q/\overline{W}_a$ vary along the span as shown in Fig. 3. Reduced frequencies of blade force on the blade due to an inflow distortion in cases No. 1 and No. 2 are calculated as $K_1 = 0.136\,q$ and $k_2 = 0.272\,q$, respectively. The pure tone acoustic power has been computed for different combinations of the circumferential mode number q and the radial distribution of the inflow distortion. In order to clarify the three-dimensional character and the accuracy of available two-dimensional theory, the results are compared with those of the strip theory method and the quasi three-dimensional method.

The finite series approximation of $L = 7$ and $M = 6$ were used for the calculations in this paper. In accordance with the increase of circumferential wave number q, the number of propagating modes (n,l) increases, and therefore the accuracy of the calculation of the $KT\binom{p}{k}$ term in equation (15) seems to decrease. In the three-dimensional calculation, the degree of accuracy seems to be greater than in the two-dimensional calculation, because the three-dimensional calculation has three-dimensional effects in the radial direction. So the calculation for a large number of propagating acoustic modes will require an increase in M.

Acoustic Power Variation with Circumferential Mode Number of Inflow Distortion

In Fig. 4, the dimensionless total acoustic powers from the 3-D calculation of the upstream and downstream propagating sound waves are plotted against the circumferential mode number q of the inflow distortion. The coefficient A_q in equation (16-1) was held constant over all values of q and the radius. In this section, we discuss the numerical results for the noncompact source case. The dimensionless acoustic power at q = 10 agrees with the Namba's results.[1] However, acoustic power levels at other values of q are different from Namba's results, because in Namba's calculation the reduced frequency is assumed as constant without regard to the variation of q. In the upper part of Fig. 4, the variation of the generated acoustic modes with the inflow distortion mode number q is shown. In the notation (ν_1, l) ν_1 corresponds to the harmonic number of the pure tone and l corresponds to the radial mode number of the acoustic mode. Therefore the circumferential mode number of the acoustic mode n is calculated with the equation $n = \nu_1 N - q$ where N is the blade number and q is the circumferential mode number of the inflow distortion.

Figure 4 shows that the number of acoustic modes increases with an increase in q. The acoustic powers of both upstream and downstream propagating sound waves are largest at about q = 30. This region of large acoustic power corresponds to a large number of 1st harmonic acoustic modes. In Fig. 4, it is seen that the total acoustic power of downstream propagating waves is higher than that of upstream propagating waves in the whole range of q.

Figure 5 shows the variation of fundamental pure tone component with circumferential wave number q of inflow distortion for case No. 1. For values of q less than 20, the fundamental tone acoustic power level of downstream propagating waves is higher than that of upstream propagating waves, but for values of greater than 20, this tendency is reversed. Total acoustic power and the acoustic power of the fundamental pure tone for case No. 2 are shown in Figs. 6 and 7. The total acoustic power radiated downstream is higher than that radiated upstream, while for the fundamental pure tone the downstream acoustic power is sometimes lower and sometimes higher than the upstream acoustic power.

Compact and Noncompact Sources

In Figs. 4 to 7, comparisons are made between the compact source prediction based on distributed sources only along a line in the spanwise direction (compact source) and a rigorous prediction based on distributed sources along both the airfoil chord and span (noncompact) for the upstream and downstream propagating sound waves. The divergence of the compact and noncompact source predictions in both the upstream and downstream propagation cases is considerable, especially in the lower reduced frequency range for small values of q. This tendency is similar to that observed by Kaji[12] in a two-dimensional cascade. The maximum acoustic power difference is 15 dB in the upstream case and 6 dB in the downstream case. The degree of difference decreases as the reduced frequency of the blade forces increases.

At the higher reduced frequencies, the unsteady forces on the blade are concentrated near the leading edge and so the phase variation of source in the chordwise direction is small. In addition, in the downstream direction, the wave length of sound is stretched due to fluid flow and therefore the ratio of wave length of sound to the chord length, a retarded time effect, is smaller than in the upstream case. Therefore, the difference in acoustic power between noncompact and compact sources is less noticeable in downstream case (see Fig. 5).

In the case of the fundamental tone (Fig. 5), the downstream acoustic power predicted by the compact source model is higher by a maximum of 7 dB than that of the noncompact source model and they approach one another in the higher source reduced frequency range. In the upstream case, the acoustic power level of the compact source prediction is considerably higher than that of the noncompact source prediction in the low reduced frequency range, but in the higher reduced frequency range, the acoustic power of the latter is higher than that of the former by several dB.

Figures 6 and 7 for case No. 2 also show that the acoustic power difference between compact and noncompact sources is smaller than in case No. 1, but still appreciable.

Acoustic Power Variation Due to Inflow Distortion Radial Distribution

Figures 8(a) and (b) show the acoustic power variation of the fundamental tone for upstream and downstream propagation. The calculations were for case No. 1 using the 3-D model. In these figures, acoustic powers for 5 cases of inflow distortion radial distribution are shown. The 5 cases are for inflow distortions with radial extents of 8, 25, 42, 67 and 100 percent of the span starting from the blade tip (see sketch in Fig. 8). These figures show that at low values of q, all of the upstream acoustic power is generated by the outer 25 percent of blade-inflow distortion interaction. At higher values of q, the 25 percent of blade-inflow distortion interaction still accounts for over half of the acoustic power. For the downstream wave a similar behavior was observed that involved the 42 percent of blade-inflow distortion interaction.

Modal Structure

Figures 9 and 10 show the variation of radial mode level for the fundamental pure tone noise for various values of q for both cases No. 1 and No. 2. It is seen that the acoustic power in the first radial mode is generally higher than that in the second radial mode.

In the case of upstream propagation, for case No. 1 (Fig. 9(a)) the acoustic power of the first radial mode is higher than second radial mode, by more than 7 dB for q less than 40. In case No. 2, (Fig. 10(a)) the second radial mode level is close to the first radial mode at $q = 12$ and 16, however, for all other values of q, the former is lower by about 5 dB than the latter.

In the case of downstream propagation (Fig. 9(b)) case No. 1 shows that the second radial mode level is lower by more than 3 dB than first radial mode level. Other radial more levels are lower yet than second radial mode level. In case No. 2 (Fig. 10(b)) the second radial mode level is lower than the first radial component level except in the range of high reduced frequency. Therefore, in almost the entire range of q and for both upstream and downstream cases, it seems that only the first radial mode might be enough for acoustic liner designs if suppression requirements are modest.

Accuracy of Two-Dimensional Method for Pure Tone Fan Noise Prediction

Comparisons are made of the acoustic powers calculated from the three-dimensional method (3-D), the two-dimensional method (2-D) and the quasi three-dimensional method (quasi 3-D), in order to clarify the three-dimensional effects and the accuracy of the two-dimensional method for fan noise prediction. Figure 11 is for case No. 1 and Fig. 12 is for case No. 2.

Numerical results for both upstream and downstream total acoustic power for case No. 1 (Figs. 11(a) and (b)) show that the acoustic power difference between the two-dimensional and three-dimensional calculation is less than 3 dB. The quasi three dimensional calculation results based upon the two-dimensional unsteady force are as close to the 3-D results as are the 2-D results.

Results for the fundamental pure tone (Figs. 11(c) and (d)) show that the level differences between 2-D (also quasi 3-D) and 3-D are smaller than for the total acoustic power. This is true for both the upstream and downstream waves.

For case No. 2, Fig. 12(a) shows the upstream total acoustic power difference between 3-D and 2-D to be about 5 dB at some values of q, but the acoustic power difference between 3-D and quasi 3-D is less than 4 dB. For the downstream wave (Fig. 12(b)), the total acoustic power difference is generally 1 dB or less in the region between $q = 8$ and $q = 24$. Figures 12(c) and (d) show similar close agreements for the fundamental tone.

The survey based on the above data indicates that the quasi 3-D method may be used for pure tone fan noise prediction with an acoustic power estimation error generally less than ±2 dB.

Comparison of Modal Structure Between 3-D and Quasi 3-D Methods

Figure 13 shows the comparison between modal structure of the fundamental pure tone based on 3-D and that based on quasi 3-D methods. Figures 13(a) and (b) are for case No. 1 and show the upstream and downstream cases, respectively, while, Figs. 13(c) and (d) are for case No. 2. In both cases, No. 1 and No. 2, the agreement of acoustic powers of corresponding acoustic modes between 3-D and quasi 3-D methods is good. In both rotor cases, the acoustic power difference of corresponding acoustic modes is less than 3 dB, and in the region of low reduced frequency, the power difference approaches zero. In accordance with these numerical results, the quasi 3-D method also seems to be adequate for acoustic modal structure prediction in the three-dimensional annular fan -- inflow distortion interaction problem.

Concluding Remarks

Comparisons are made among the predictions based on three-dimensional theory, strip theory and quasi three-dimensional theory, in order to clarify the accuracy of available two-dimensional theory for the prediction of pure tone fan noise due to the interaction of inflow distortion with a subsonic annular blade row. The theories were derived with the aid of an unsteady three-dimensional lifting surface theory developed by Namba.[1] Both compact and noncompact sources were considered. Several numerical calculations were carried out and the following results were obtained.

1. The compact source prediction in a three-dimensional annular blade row can overestimate the upstream radiation by 15 dB and the downstream radiation by 6 dB. The degree of overestimation depends on blade row characteristics and reduced frequency and interblade phase due to inflow distortion. This result implies that noncompact source effects must be considered.

2. The upstream radiation seems to depend heavily on the tip region of blade-inflow distortion interaction for both upstream and downstream cases. The extent of spanwise contribution to the sound was greater in the downstream case than in the upstream case.

3. The numerical results show that for acoustic liner design the consideration of only the first radial acoustic mode is enough when only modest suppression is needed.

4. Strip theory and quasi three-dimensional theory based on the two-dimensional calculation of unsteady forces are reasonably adequate for fan noise prediction. The quasi three-dimensional method is more accurate for acoustic power and for modal structure prediction, with an acoustic power estimation error of ±2 dB or less.

Acknowledgement

The author conducted this work at NASA-Lewis Research Center as a National Research Council - NASA-Lewis Associate. The author thanks Dr. Charles E. Feiler, Dr. Marvin E. Goldstein and many other members of NASA-Lewis Research Center, who gave him much encouragement and advice.

Appendix - Kernel Function KT_k

The kernel function KT_k is composed of the three parts $KT_k^{(P)}$, $KT_k^{(S)}$, and $KT_k^{(R)}$, which are given as follows:

$$KT_k^{(P)}(r,\theta_o,z-\zeta)$$

$$= \sum_{\nu=\nu-}^{\nu+} \sum_{l=0}^{L-1} \Big(e^{-i\omega(z-\zeta)} \cdot e^{in\theta_o} \cdot \{-[1+\mathrm{sgn}(z-\zeta)]\} \cdot BK_{na}$$

$$+ [\mathrm{sgn}(z-\zeta)\cdot BK_{na} + i\cdot BK_{nb}]\, e^{i\chi_1 + in\chi_2} \cdot e^{-\Omega_{n,l}|z-\zeta|}\Big), \quad \text{(A1)}$$

$$KT_k^{(S)}(r,\theta_o,z-\zeta)$$

$$= e^{-i\omega(z-\zeta)} \sum_{l=0}^{L-1} \left[-e^{i\sigma\theta_o}\cdot BK_{1l} - \omega\cdot H_3(\theta_o,N,\sigma)\cdot BK_{2l}\right]$$

$$+ \sum_{l=0}^{L-1} e^{i\chi_1}\Big\{[\mathrm{sgn}(z-\zeta)\cdot BK_{1l} + iBK_{3l}]\cdot H_1(\chi_3 - i\chi_2;N,\sigma)e^{\chi_4}$$

$$+ [\mathrm{sgn}(z-\zeta)\cdot BK_{1l} - i\cdot BK_{3l}]\cdot H_1(\chi_3 + i\chi_2;N,-\sigma)\, e^{-\chi_4}\Big\}$$

$$+ \sum_{l=0}^{L-1} \omega\cdot e^{i\chi_1}\Big\{[-\mathrm{sgn}(z-\zeta)\cdot BK_{2l} + i\cdot BK_{4l}]$$

$$\times H_2(\chi_3 - i\chi_2;N,\sigma)\, e^{\chi_4} + [\mathrm{sgn}(z-\zeta)\cdot BK_{2l} + i\cdot BK_{4l}]$$

$$\times H_2(\chi_3 + i\chi_2;N,-\sigma)\, e^{-\chi_4}\Big\} - [1+\mathrm{sgn}(z-\zeta)]\cdot e^{i\omega(z-\zeta)}$$

$$\times \sum_{\substack{\nu=\nu-\\ \nu\neq 0}}^{\nu+} e^{in\theta_o}\left(BK_{1l} - \frac{\omega}{n}\cdot BK_{2l}\right) - \sum_{\substack{\nu=\nu-\\ \nu\neq 0}}^{\nu+} e^{i(\chi_1 + n\chi_2)}$$

$$\times \sum_{l=0}^{L-1}\Big\{[\mathrm{sgn}(z-\zeta)\cdot BK_{1l} + i\cdot\mathrm{sgn}(n)\cdot BK_{3l}] - \left(\frac{\omega}{n}\right)$$

$$\times [\mathrm{sgn}(z-\zeta)\times BK_{2l} - i\cdot\mathrm{sgn}(n)\cdot BK_{4l}]\Big\}\cdot \exp(M_{n,l}|z-\zeta|), \quad \text{(A2)}$$

$$KT_k^{(R)}(r,\theta_o,z-\zeta)$$

$$= -[1+\mathrm{sgn}(z-\zeta)]\, e^{-i\omega(z-\zeta)} \sum_{\substack{\nu=-\infty\\ \nu\neq\nu- - \nu+}}^{\infty} e^{in\theta_o} \sum_{l=0}^{L-1}$$

$$\times \left(BK_{na} - BK_{1l} + \frac{\omega}{n} BK_{2l}\right) + e^{i\chi_1} \sum_{\substack{\nu=-\infty\\ \nu\neq\nu- - \nu+}}^{\infty} e^{in\chi_2} \sum_{l=0}^{L-1}$$

$$\times \Big([\mathrm{sgn}(z-\zeta)\cdot BK_{na} + iBK_{nb}]\cdot \exp(-\Omega_{n,l}|z-\zeta|)$$

$$- \Big\{\mathrm{sgn}(z-\zeta)\cdot BK_{1l} + i\cdot\mathrm{sgn}(n)\cdot BK_{3l} + \left(\frac{\omega}{n}\right)[\mathrm{sgn}(z-\zeta)\cdot$$

$$\times BK_{2l} - i\cdot\mathrm{sgn}(n)\cdot BK_{4l}]\Big\}\times \exp(M_{n,l}\cdot|z-\zeta|)\Big), \quad \text{(A3)}$$

where

$$BK_{na} \equiv \frac{1}{k_{n,l}^2 + (n\omega_T + \omega)^2} \times (FR_n\cdot C_{n,l,m} + GR_{n,l}\cdot B_{n,l,m})\cdot R_n(k_{n,l}\cdot r) \quad \text{(A4)}$$

$$BK_{nb} \equiv \frac{1}{k_{n,l}^2 + (n\omega_T + \omega)^2}\,\frac{1}{\Omega_{n,l}} \times R_n(k_{n,l}\cdot r)\ (GI_{n,l}\cdot B_{n,l,m} + FI_{n,l}\cdot C_{n,l,m}) \quad \text{(A5)}$$

$$BK_{1l} \equiv \frac{1}{K_{\infty,l}^2 + \omega_T^2}\cdot R_\infty(k_{\infty,l}\cdot r)\cdot(-AB\cdot C_{\infty,l,m} + AA\cdot B_{\infty,l,m}) \quad \text{(A6)}$$

$$BK_{2l} \equiv \left[\left(-\frac{2\omega_T}{K_{\infty,l}^2 + \omega_T^2}\cdot AB + AC\right)\cdot C_{\infty,l,m} + \left(\frac{2\omega_T}{K_{\infty,l}^2 + \omega_T^2}\, AA - AD\right)\cdot B_{\infty,l,m}\right] \times \frac{R_\infty(k_{\infty,l}\cdot r)}{K_{\infty,l}^2 + \omega_T^2} \quad \text{(A7)}$$

$$BK_{3l} \equiv \frac{1}{K_{\infty,l}^2 + \omega_T^2}\cdot R_\infty(k_{\infty,l}\cdot r)\,\frac{1}{\hat{\Omega}_{\infty,l}}\,(AE\cdot B_{\infty,l,m} + AF\cdot C_{\infty,l,m}) \quad \text{(A8)}$$

$$BK_{4l} \equiv \frac{1}{K_{\infty,l}^2 + \omega_T^2}\cdot R_\infty(k_{\infty,l}\cdot r)\left[\left(-\frac{2\omega_T}{K_{\infty,l}^2 + \omega_T^2}\,\frac{1}{\hat{\Omega}_{\infty,l}} + \frac{M_a^2\omega_T}{\beta_a^4\hat{\Omega}_{\infty,l}^3}\right) \times (AE\cdot B_{\infty,l,m} + AF\cdot C_{\infty,l,m}) + \frac{1}{\hat{\Omega}_{\infty,l}} \times (AE\cdot B_{\infty,l,m} + AH\cdot C_{\infty,l,m})\right] \quad \text{(A9)}$$

$$FR_n \equiv -n\left[\frac{n}{r} + (n\omega_T + \omega)\cdot\omega_T\cdot r\right] \quad \text{(A10)}$$

$$GR_{n,l} \equiv \frac{\omega_T}{\beta_a^2}\left[\omega_T r\cdot k_{n,l}^2 - \frac{\beta_a^2 n(n\omega_T + \omega)}{r} + M_a^2(n\omega_T + \omega)^2\omega_T r\right] \quad \text{(A11)}$$

$$GI_{n,l} \equiv \frac{\omega_T}{\beta_a^2}\left\{\frac{(n\omega_T + \omega)^2 M_a^2}{\beta_a^2}\left[\frac{n}{r} - \frac{(n\omega_T + \omega)\omega_T r M_a^2}{\beta_a^2}\right] + \left[k_{n,l}^2 - \frac{M_a^2(n\omega_T + \omega)^2}{\beta_a^2}\right]\times\left[\frac{n}{r} + \left(1 - \frac{M_a^2}{\beta_a^2}\right)(n\omega_T + \omega)\omega_T r\right]\right\} \quad \text{(A12)}$$

$$FI_{n,l} \equiv \frac{n}{\beta_a^2}\left[k_{n,l}^2\cdot r\cdot\omega_T - \frac{n(n\omega_T + \omega)}{r}\right] \quad \text{(A13)}$$

$$AA \equiv \left(\omega_T r\cdot K_{\infty,l}^2 - \frac{\beta_a^2}{r}\,\omega_T + M_a^2\omega_T^3 r\right)\frac{\omega_T}{\beta_a^2} \quad \text{(A14)}$$

$$AB \equiv \frac{1}{r} + \omega_T^2 r \tag{A15}$$

$$AC \equiv \omega_T \cdot r \tag{A16}$$

$$AD \equiv \frac{\omega_T}{\beta_a^2}\left(-\frac{\beta_a^2}{r} + 2M_a^2\omega_T^2 r\right) \tag{A17}$$

$$AE \equiv \frac{\omega_T \cdot K_{\infty,l}^2}{\beta_a^2}\left(\frac{1}{r} + \omega_T^2 r - \frac{M_a^2\omega_T^2 r}{\beta_a^2}\right) - \frac{M_a^2\omega_T^5 r}{\beta_a^4} \tag{A18}$$

$$AF \equiv \frac{1}{\beta_a^2}\left(K_{\infty,l}^2 r\cdot\omega_T - \frac{\omega_T}{r}\right) \tag{A19}$$

$$AG \equiv -\frac{3M_a^2\omega_T^4 r}{\beta_a^4} + K_{\infty,l}^2\left(1 - \frac{M_a^2}{\beta_a^2}\right)\frac{r\omega_T^2}{\beta_a^4} \tag{A20}$$

$$AH \equiv -\frac{1}{r\beta_a^2} \tag{A21}$$

$$X_1 \equiv \frac{M_a^2}{\beta_a^2}\,\omega(z - \zeta) \tag{A22}$$

$$X_2 \equiv \theta_o + \frac{1}{\beta_a^2}\,\omega_T(z - \zeta) \tag{A23}$$

$$X_3 \equiv \hat{\beta}_{\infty,l}\,|z - \zeta| \tag{A24}$$

$$X_4 \equiv \frac{1}{\hat{\beta}_{\infty,l}}\,\frac{M_a^2}{\beta_a^4}\,\omega_T\cdot\omega\cdot|z - \zeta| \tag{A25}$$

$$\hat{\beta}_{\infty,l} \equiv \frac{1}{\beta_a}\left(K_{\infty,l}^2 - \frac{M_a^2}{\beta_a^2}\,\omega_T^2\right)^{1/2} \tag{A26}$$

$$N_{n,l} \equiv -|n|\cdot\hat{\beta}_{\infty,l} + \mathrm{sgn}(n)\,\frac{M_a^2\omega\omega_T}{\beta_a^4\hat{\beta}_{\infty,l}} \tag{A27}$$

$$H_1(X;N,\sigma) \equiv 1/(e^{(N+\sigma)X} - e^{\sigma X}) \tag{A28}$$

$$H_2(X;N,\sigma) \equiv \int_X^\infty H_1(X;N,\sigma)\,dx \tag{A29}$$

$$H_3(\theta_o;N,\sigma) = H_2(-i\theta_o;N,\sigma) - H_2(i\theta_o;N,-\sigma) \tag{A30}$$

References

1. Namba, M., "Three-Dimensional Analysis of Blade Force and Sound Generation for an Annular Cascade in Distorted Flows," Journal of Sound and Vibration, Vol. 50, Feb. 1977, pp. 479-508.

2. Namba, M., "Lifting Surface Theory for a Rotating Subsonic or Transonic Blade Row," Aeronautical Research Council, R&M No. 3740, 1974.

3. Whitehead, D. S., "Vibration and Sound Generation in a Cascade of Flat Plates in Subsonic Flow," Aeronautical Research Council, R&M, No. 3685, 1972.

4. Mani, R., "Isolated Rotor Noise Due to Inflow Distortion or Turbulence," NASA CR-2479, 1974.

5. Goldstein, M. E., Dittmar, J. H., and Gelder, T. F., "Combined Quadrupole-Dipole Model for Inlet Flow Distortion Noise from a Subsonic Fan," NASA TN D-7676, 1974.

6. Goldstein, M. E., Rosenbaum, B. M., and Albers, L. U., "Sound Radiation from a High-Speed Axial-Flow Fan Due to the Inlet Turbulence Quadrupole Interaction," NASA TN D-7667, 1974.

7. Pickett, G. F., "Effects of Non-Uniform Inflow on Fan Noise," Journal of Acoustical Society of America," Vol. 55, Suppl., Session B5, 1974, p. S4.

8. Hanson, D. B., "Spectrum of Rotor Noise Caused by Atmospheric Turbulence," Journal of the Acoustical Society of America, Vol. 56, July 1974, pp. 110-126.

9. Cumpsty, N. A., and Lowrie, B. W., "The Cause of Tone Noise Generation by Aeroengine Fans at High Subsonic Tip Speeds and the Effect of Forward Speed," ASME Paper 73-WA/GT-4, Nov. 1973.

10. Feiler, C. E., and Groeneweg, J. F., "Summary of Forward Velocity Effects on Fan Noise," AIAA Paper 77-1319, Oct. 1977.

11. Rice, E. J., "Spinning Mode Sound Propagation in Ducts with Acoustic Treatment," NASA TN D-7913, 1975.

12. Kaji, S., "Noncompact Source Effect on the Prediction of Tone Noise from a Fan Rotor," AIAA Paper 75-446, Mar. 1975.

13. Hanson, D. B., "Unified Analysis of Fan Stator Noise," Journal of the Acoustical Society of America, Vol. 54, Dec. 1973, pp. 1571-1591.

14. Goldstein, M. E., "Aeroacoustics," McGraw-Hill, New York, 1976.

15. Graham, J. M. R., "Lifting Surface Theory for the Problem of an Arbitrarily Yawed Sinusoidal Gust Incident on a Thin Aerofoil in Incompressible Flow," Aeronautical Quarterly, Vol. 21, May 1970, pp. 182-198.

16. Tyler, J. M., and Sofrin, T. G., "Axial Flow Compressor Noise Studies," Society of Automotive Engineers Transactions, Vol. 70, 1962, pp. 309-332.

17. McCune, J. E., "The Three-Dimensional Flow Field of an Axial Compressor Blade Row - Subsonic, Transonic, and Supersonic," Doctoral Thesis in Cornell University, Feb. 1958.

18. Morfey, C. L., "Sound Transmission and Generation in Ducts with Flow," Journal of Sound and Vibration, Vol. 14, Jan. 1971, pp. 37-55.

TABLE I. - FAN PARAMETERS

	Case 1	Case 2
Rotor blade number, N	40	15
Axial chord length, dimensionless, C_a	0.05498	0.25836
Rotor speed/axial flow speed, ω_r	2.474	0.627
Rotor relative Mach number, M_r	0.934	0.865
Axial flow Mach number, M_a	0.35	0.596
Hub/tip ratio, h	0.4	0.46

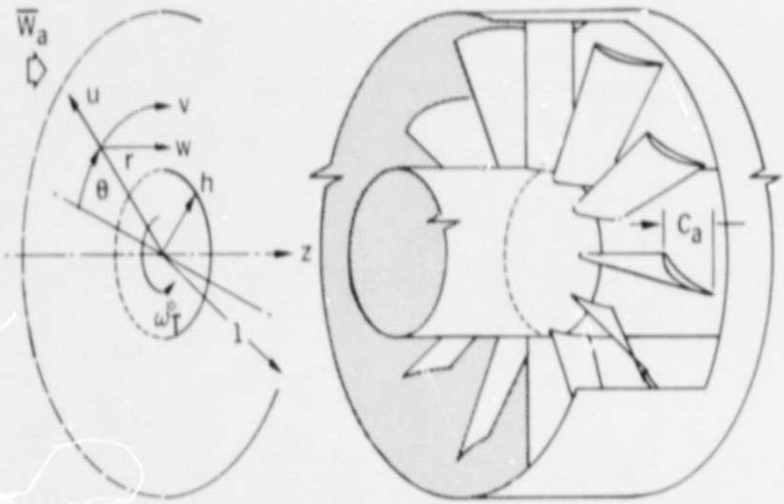

Figure 1. - Analytical model and cylindrical coordinate system.

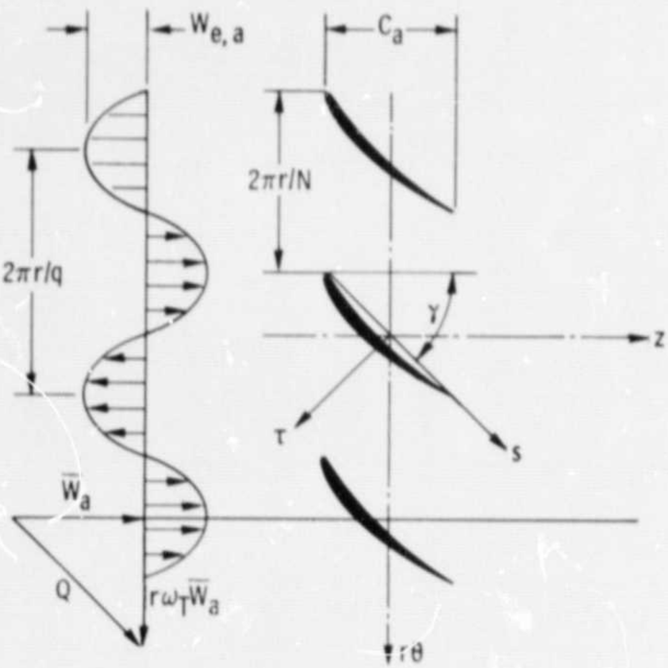

Figure 2. - The velocity distribution for inflow distortion model at a constant radius plane.

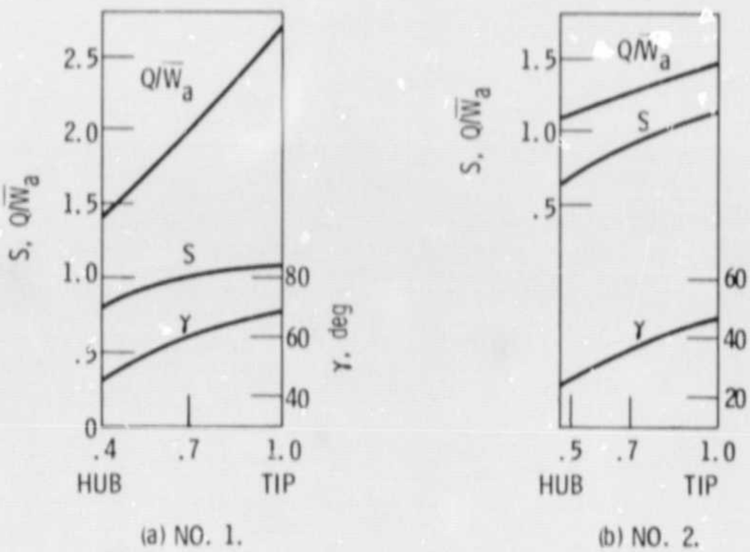

Figure 3. - Radial variations of stagger angle γ, pitch-chord ratio S and velocity ratio $Q/\overline{W}_a$ of the rotor.

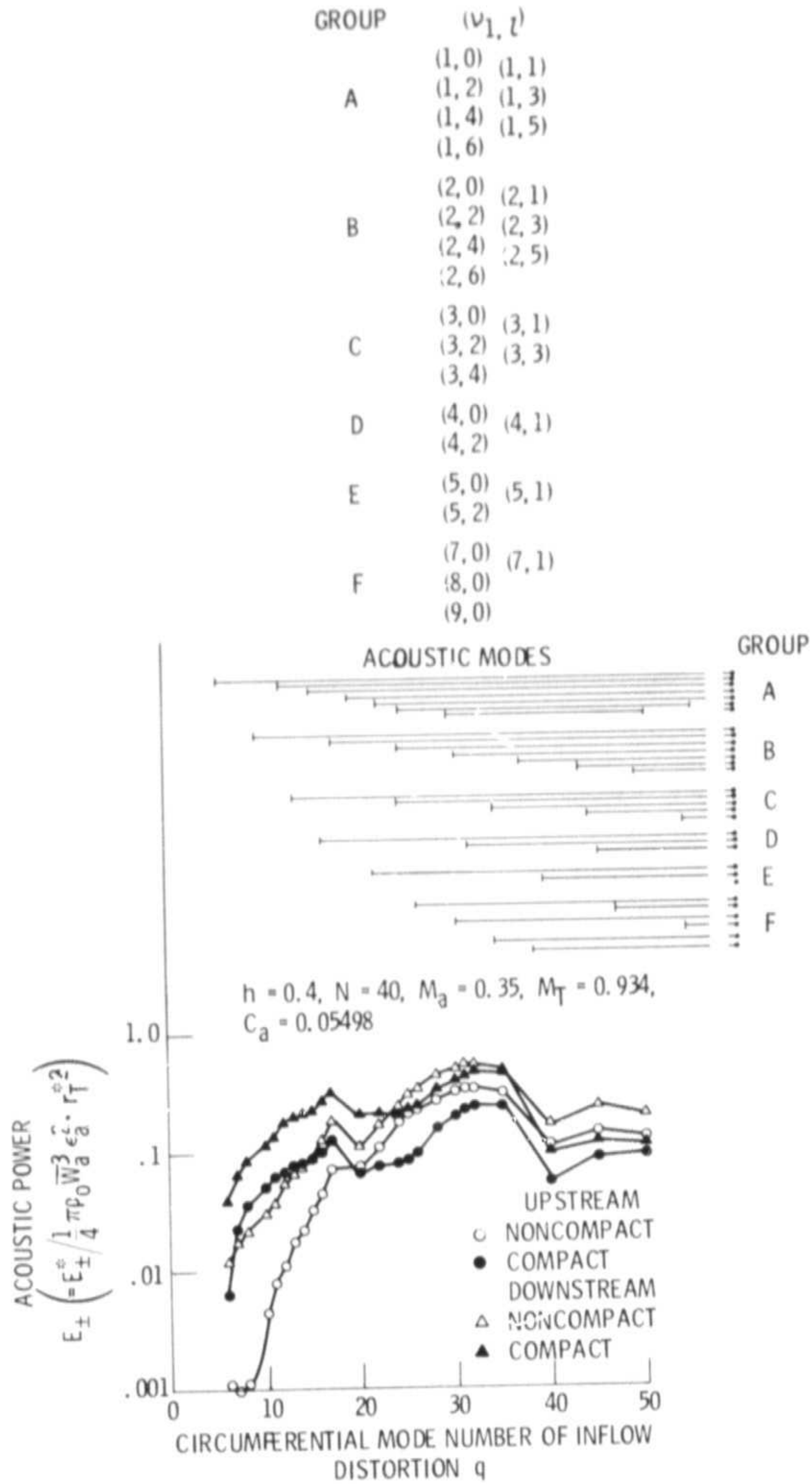

Figure 4. - Variation of total acoustic power with inflow distortion circumferential mode number, case no. 1. (Uniform radial distribution of inflow distortion.)

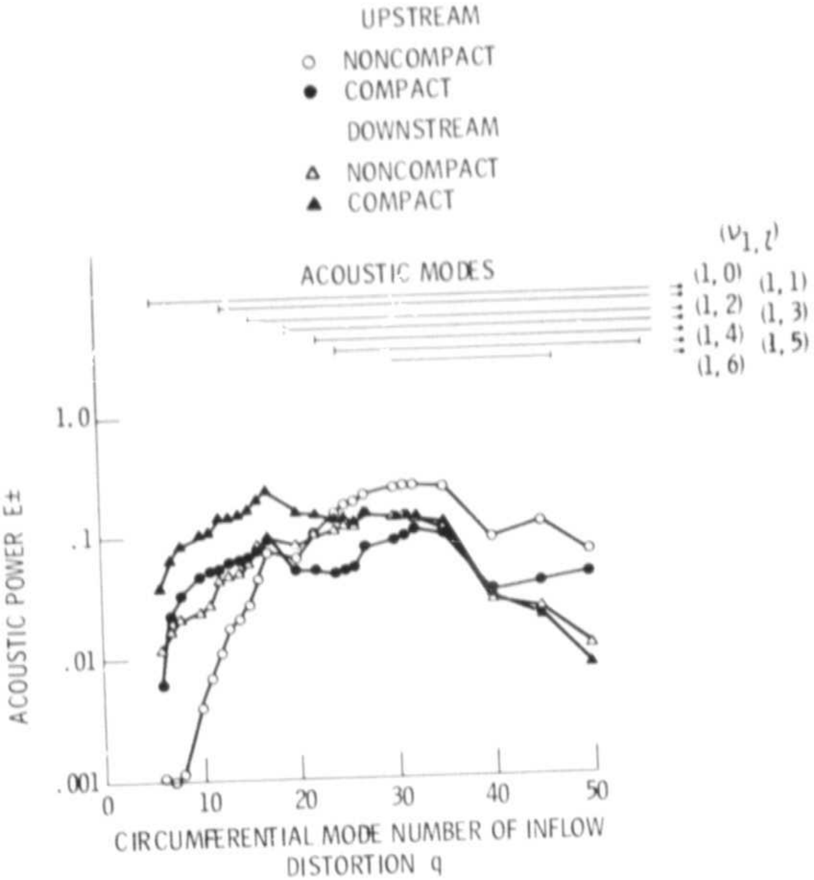

Figure 5. - Variation of fundamental pure tone noise with inflow distortion circumferential mode number, case no. 1. (Uniform radial distribution of inflow distortion.)

GROUP	(ν_1, l)	
A	(1, 0)	(1, 2)
B	(2, 0)	(2, 1)
	(2, 2)	(2, 3)
	(2, 4)	(2, 5)
	(2, 6)	
C	(3, 0)	(3, 1)
	(3, 2)	(3, 3)
	(3, 4)	(3, 5)
D	(4, 0)	(4, 1)
	(4, 2)	(4, 3)
	(4, 4)	
	(5, 0)	(5, 1)
	(5, 2)	(5, 3)
E	(6, 0)	(6, 1)
	(6, 2)	
	(7, 0)	(7, 1)

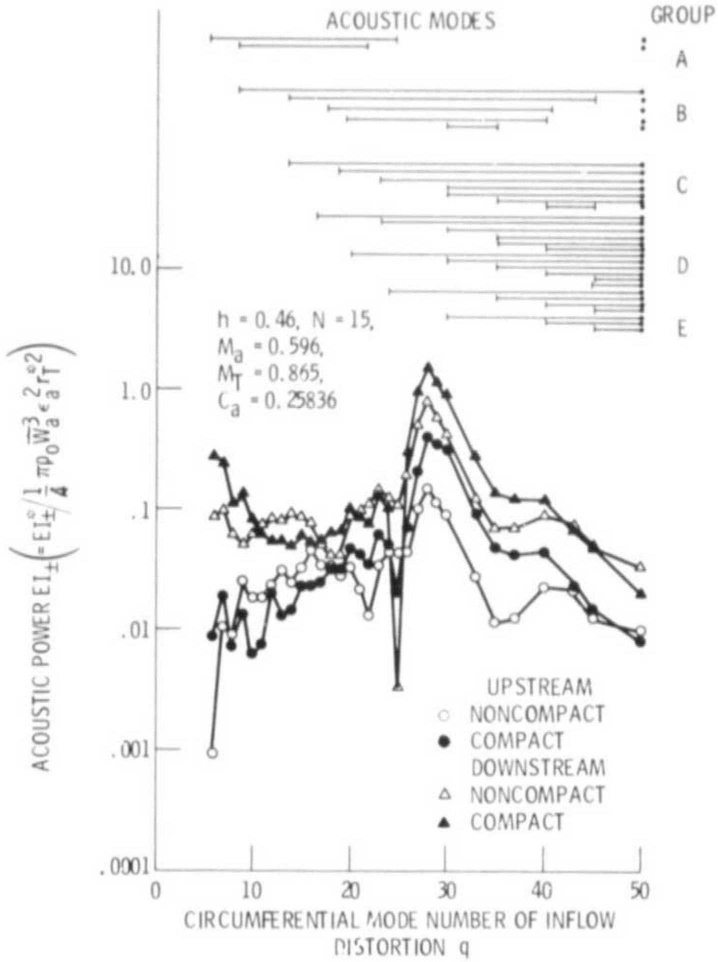

Figure 6. - Variation of total acoustic power with inflow distortion circumferential mode number q, case no. 2. (Uniform radial distribution of inflow distortion.)

E-9613

ORIGINAL PAGE IS
OF POOR QUALITY

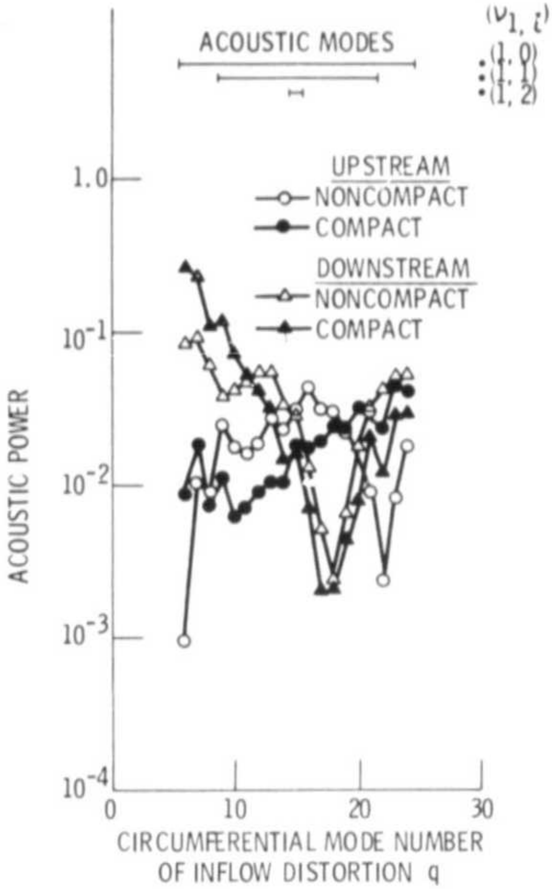

Figure 7. - Variation of fundamental pure tone noise with inflow distortion circumferential mode number q, case no. 2 (uniform radial distribution of inflow distortion).

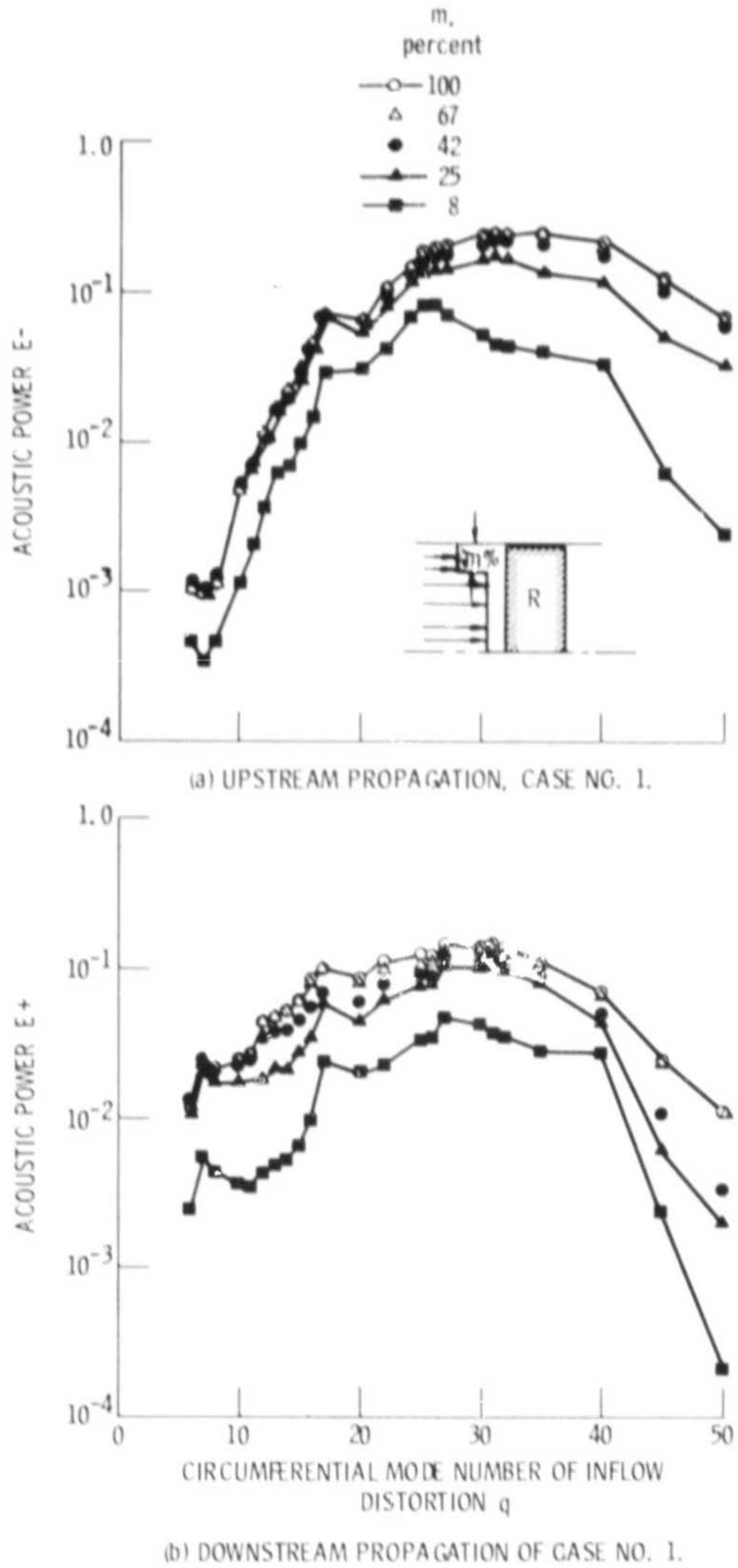

(a) UPSTREAM PROPAGATION, CASE NO. 1.

(b) DOWNSTREAM PROPAGATION OF CASE NO. 1.

Figure 8. - Variation of fundamental pure tone noise with inflow distortion radial distribution.

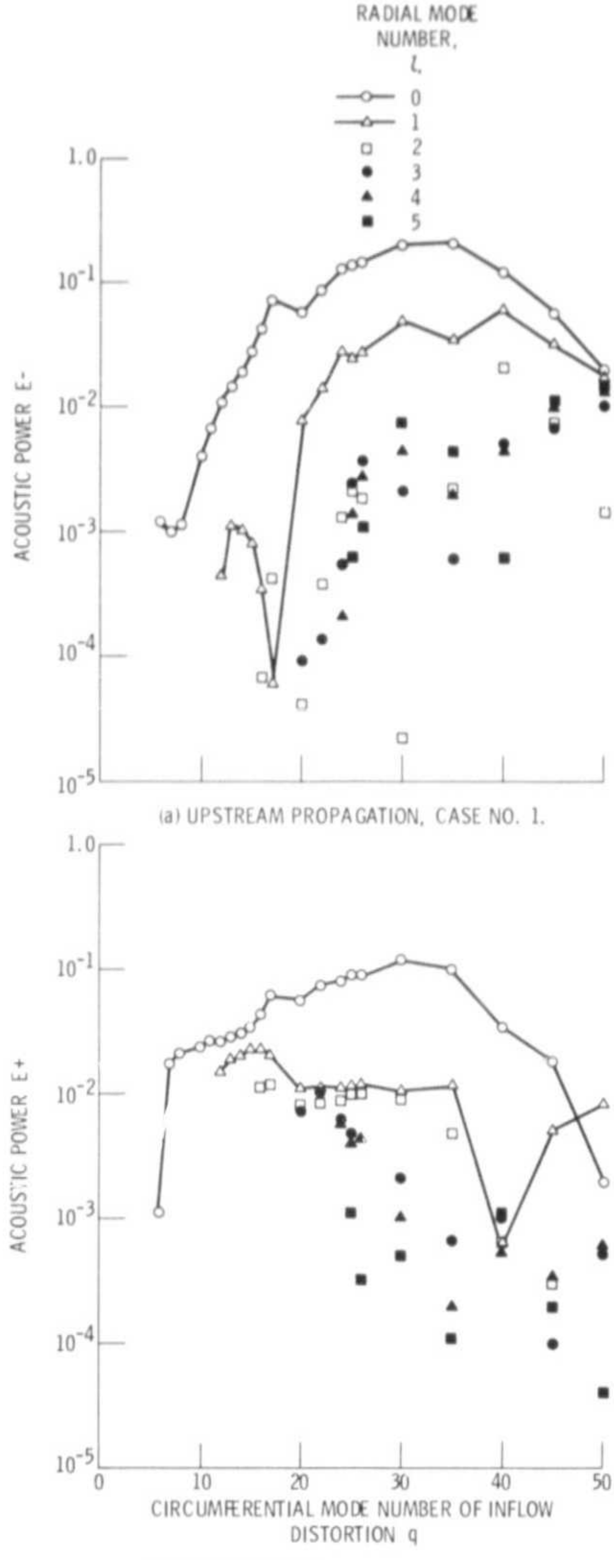

Figure 9. - Variation of radial mode levels of fundamental pure tone noise with inflow distortion circumferential mode number. (Uniform radial distribution of inflow distortion.)

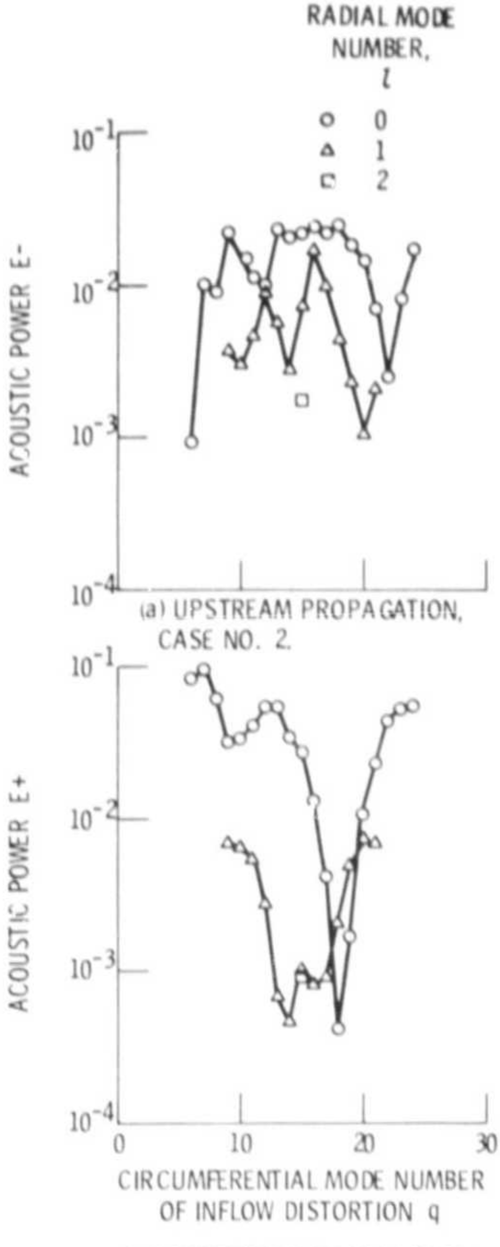

Figure 10. - Variation of radial mode levels of fundamental pure tone noise with inflow distortion circumferential wave number. (Uniform radial distribution of inflow distortion.)

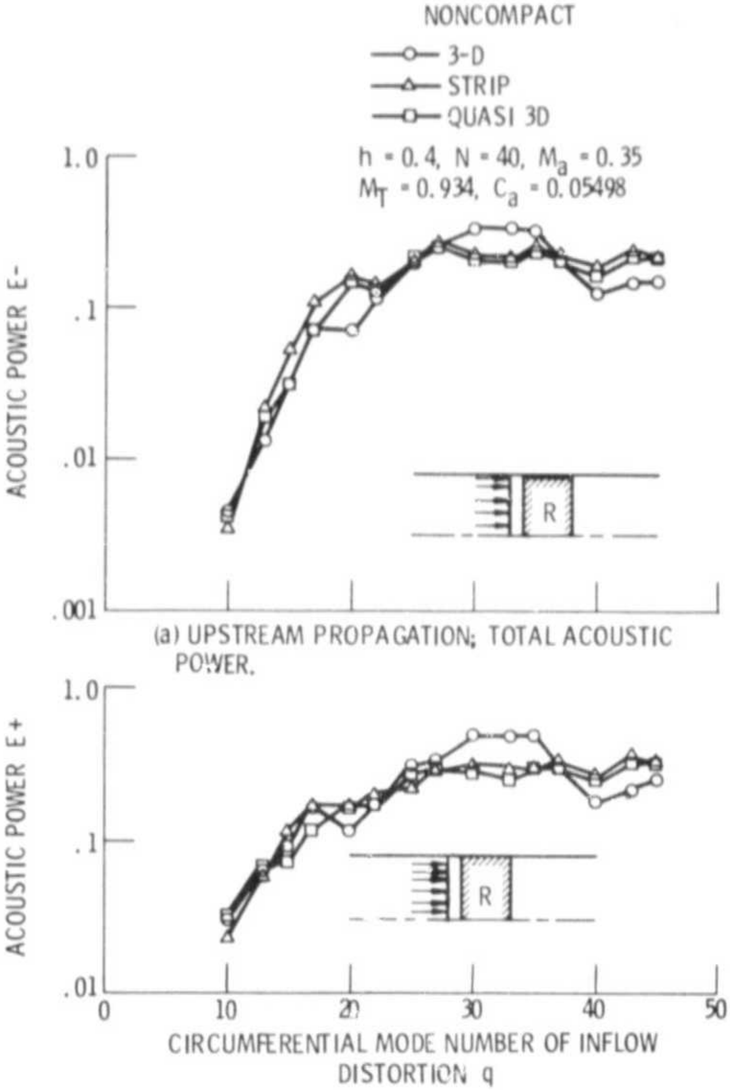

(b) DOWNSTREAM PROPAGATION; TOTAL ACOUSTIC POWER.

Figure 11. - Comparison of acoustic powers among 3-D method, 2-D method, and quasi 3-D method - case 1.

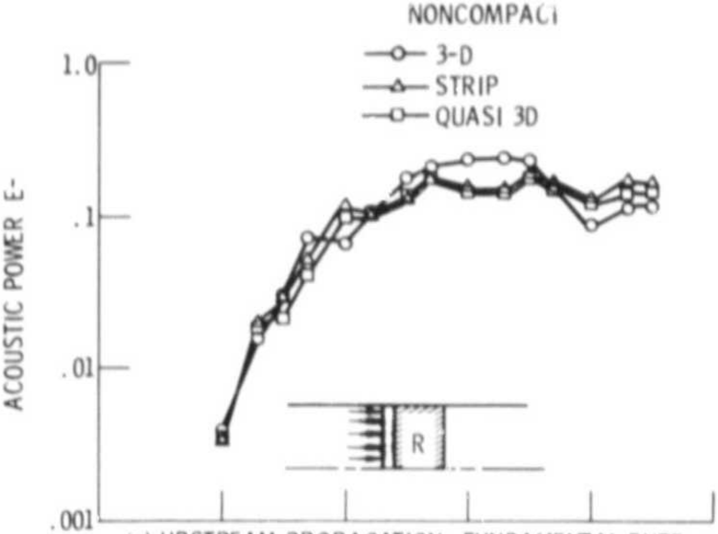

(c) UPSTREAM PROPAGATION; FUNDAMENTAL PURE TONE.

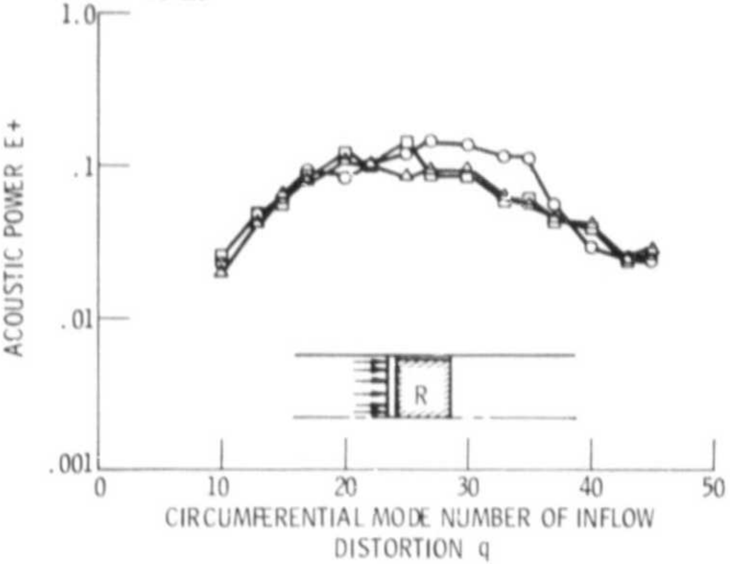

(d) DOWNSTREAM PROPAGATION; FUNDAMENTAL PURE TONE.

Figure 11. - Concluded.

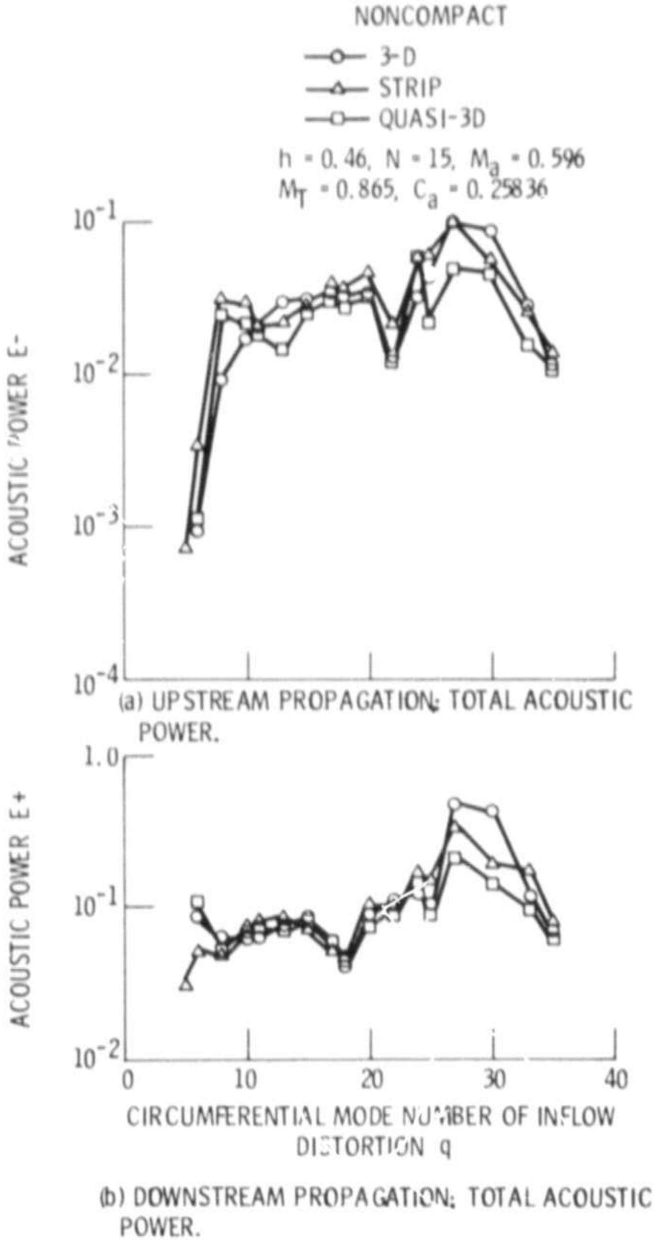

Figure 12. - Comparison of acoustic powers among 3-D method, 2-D method, and quasi 3-D method - case 2.

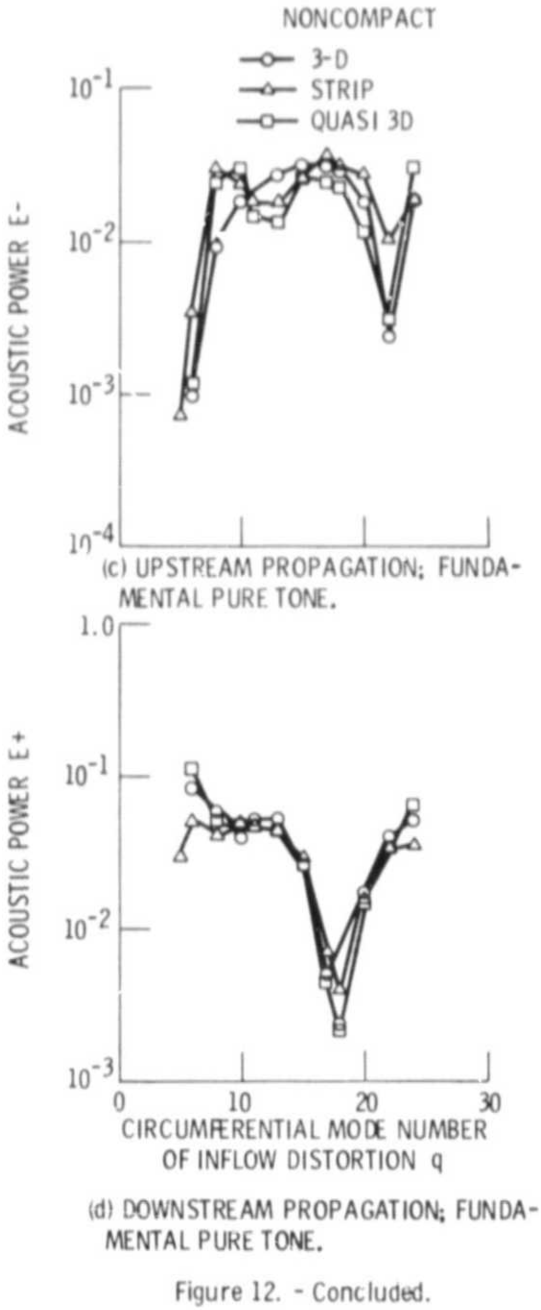

Figure 12. - Concluded.

ORIGINAL PAGE IS OF POOR QUALITY

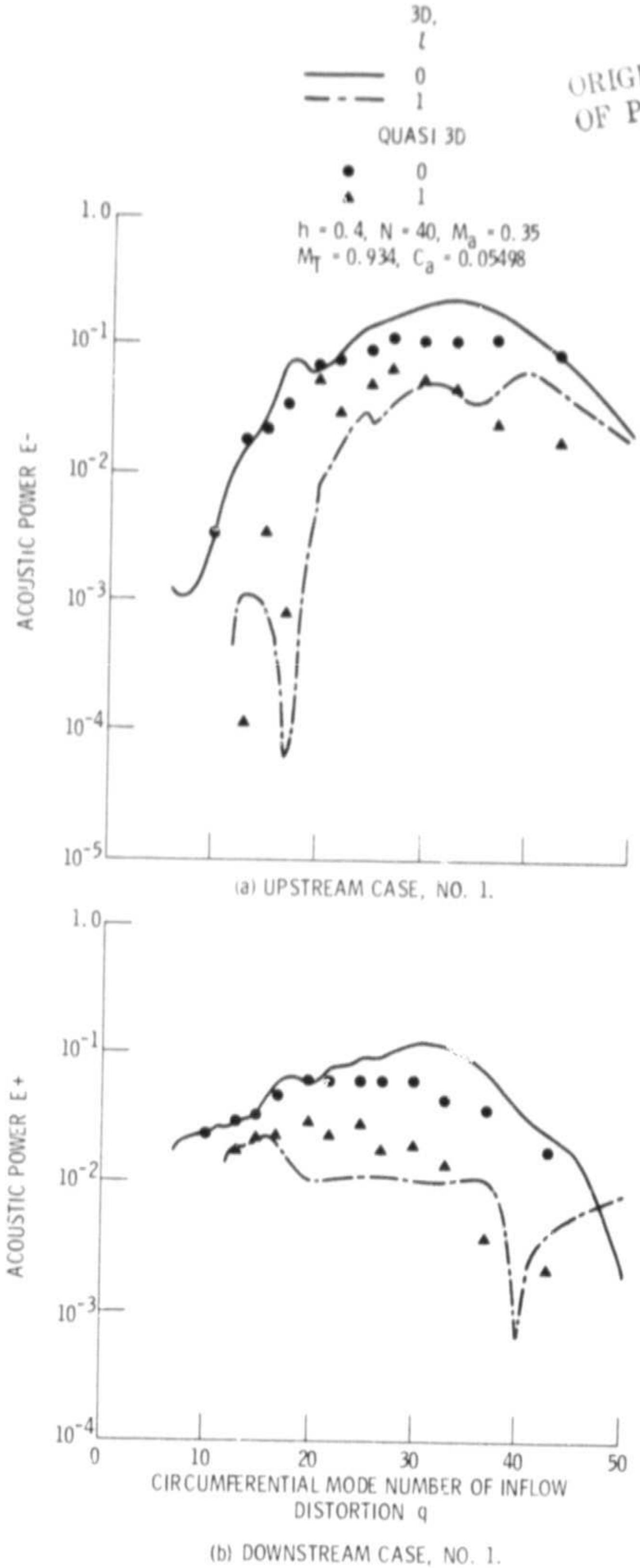

Figure 13. - Comparison of modal structure of fundamental pure tone noise between 3-D method and quasi 3-D method.

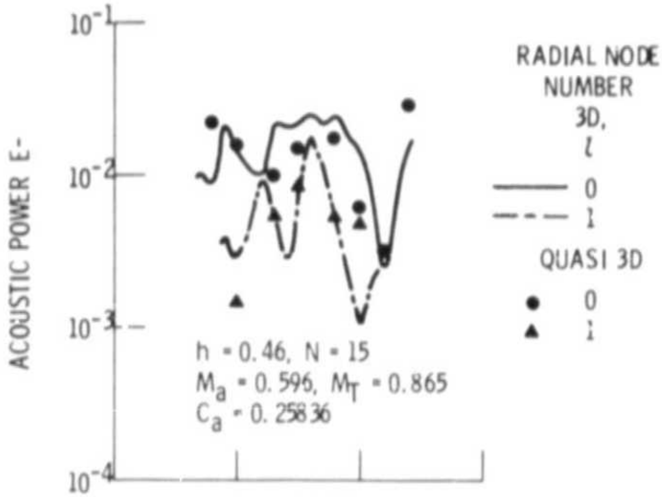

(c) UPSTREAM CASE, NO. 2.

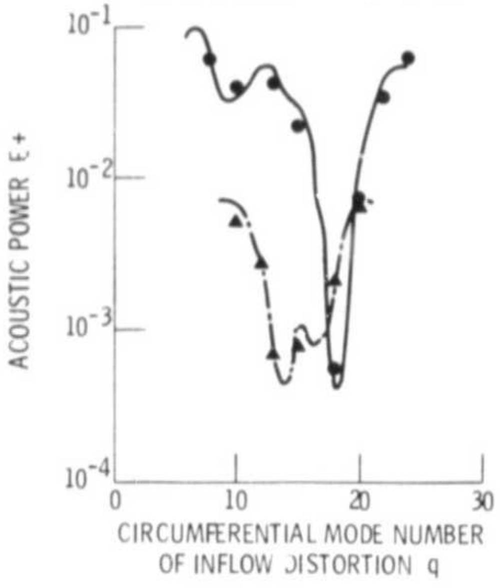

(d) DOWNSTREAM CASE, NO. 2.

Figure 13. - Concluded.